Stabilized spectral element computations of high Reynolds number incompressible flows

Chuanju Xu
Dpt of Mathematics, Xiamen University, Xiamen, China
Richard Pasquetti *
Lab. J.A. Dieudonné, UMR CNRS 6621,
Université de Nice-Sophia Antipolis, Nice, France

November 18, 2003

Abstract

The possibility of using the spectral vanishing viscosity method for the spectral element computation of high Reynolds number incompressible flows is investigated. An exponentially accurate stabilized formulation is proposed and then applied to the computation of the 2D wake of a cylinder. Such a formulation can be easily implemented in existing spectral element solvers, since only modifying the computation of the viscous term while preserving the symmetry of the corresponding bilinear form.

1 Introduction

High Reynolds number flows are difficult to compute, especially when using spectrally accurate numerical schemes. This directly results from the fact that spectral approximations are much less numerically diffusive than low-order ones, so that the non artificially dissipated energy accumulates at the high spatial frequencies and finally leads to the divergence of the computations. One way to overcome this difficulty is to use stabilization techniques, but then the spectral accuracy of the algorithm is generally destroyed. This is e.g. particularly obvious for approaches which essentially consist in adding

*Corresponding author

some $O(h^r)$ hyper viscous term, in the spirit of [14]. For a long time filtering techniques have also been proposed to overcome the stability problem. In the frame of spectral element approximations it is however essential to preserve the inter-element continuity, as discussed in [2]. One of the most recent advances in this field has been proposed in [6], (and discussed in [16]) where a spectrally accurate approach is applied to the direct numerical simulation (DNS) of high Reynolds number flows.

Here we essentially focus on the spectral vanishing viscosity (SVV) method, which appears to be an efficient stabilization technique possessing the property to preserve the spectral accuracy. It was initially developed for the resolution of hyperbolic equations using standard Fourier spectral methods [21]. The non-periodic case was then considered in the frame of the spectral Legendre approximation [13]. Further refinements have been recently suggested, through the use of a spectral hyper-viscous (rather than a viscous) term or through the redefinition of the stabilization term [8]. Recently, it has also been suggested to use the SVV method, in its first formulation, for the large-eddy simulation of turbulent flows [10, 15].

In this paper, our goal is to check the capabilities of the SVV method, in terms of accuracy and stability, when it is implemented in a Navier-Stokes spectral element solver.

First we show how to implement the SVV method in the frame of a spectral element approximation. The fact that complex multidimensional geometries and vector valued functions are concerned make this point non trivial, so that one cannot yet consider that a standard way to implement the SVV method already exists. Moreover, we suggest using an approximate form which can be efficiently implemented in any spectral element solver. The advantage of such an approximate form is that the computational cost per iteration (time-step if a direct solver is used) is roughly the same with and without SVV stabilization.

Second we consider an elliptic equation solved by a steep analytical solution and show that the convergence results obtained with the spectral element approximation are coherent with those obtained in the 1D periodic case, when using Fourier expansions. A detailed study of the influence of the SVV tuning parameters on the convergence rates is provided. Then we consider the so-called "Kovasznay flow", which is an exact solution of the incompressible Navier-Stokes equations, and again check the capabilities of the SVV method.

Third, in order to numerically demonstrate the stabilization property of the method, we compute 2D wakes of a cylinder, at Reynolds numbers up to $Re = 1000$, i.e. much higher than the critical value associated with the 2D-3D transition ($Re \approx 190$).

Finally, we conclude by emphasizing the interest in the SVV-stabilized spectral element method (SEM) for the large-eddy simulation (LES) of turbulent flows.

2 Stabilized spectral element formulation

The flow of an incompressible Newtonian fluid is governed by the "incompressible Navier-Stokes equations". For an unsteady flow in a domain Ω they read:

$$\left\{ \begin{array}{rl} D_t \boldsymbol{u} - \nu \nabla^2 \boldsymbol{u} + \nabla p &= \boldsymbol{s} \quad in\, \Omega \times R^+ \\ \nabla \cdot \boldsymbol{u} &= 0 \quad in\, \Omega \times R^+ \end{array} \right. \tag{1}$$

where $\boldsymbol{u}$, p and $\boldsymbol{s}$ denote the velocity, pressure and source term respectively, $D_t \boldsymbol{u}$ the material (Lagrangian) derivative of $\boldsymbol{u}$ with respect to time t and ν the dimensionless viscosity (the inverse of the Reynolds number). The unsteady Navier-Stokes equations must be associated to appropriate initial and boundary conditions, e.g. $\boldsymbol{u}(t=0) = 0$ (fluid at rest) and $\boldsymbol{u}|_\Gamma = 0$ (no-slip condition at the boundary Γ of Ω), in order to set up a well-posed problem that one can then try to solve numerically.

If (i) complex geometries are considered and (ii) high accuracy is desired, then the SEM is well suited (see e.g. [11]). The spectral element approximation of the weak form of the incompressible Navier-Stokes equations yields the following semi-discrete variational problem, to be solved at each time-step after the time-discretization: Find $\boldsymbol{u}_N \in \boldsymbol{X}_N$ and $p_N \in M_N$ such that

$$\left\{ \begin{array}{rl} (D_t \boldsymbol{u}_N, \boldsymbol{v}_N) + \nu(\nabla \boldsymbol{u}_N, \nabla \boldsymbol{v}_N) - (\nabla \cdot \boldsymbol{v}_N, p_N) &= (\boldsymbol{s}_N, \boldsymbol{v}_N)\ ,\ \forall \boldsymbol{v}_N \in \boldsymbol{X}_N \\ (\nabla \cdot \boldsymbol{u}_N, q_N) &= 0\ ,\ \forall q_N \in M_N \end{array} \right. \tag{2}$$

where $\boldsymbol{u}_N$, p_N and $\boldsymbol{s}_N$ denote the spectral element approximations of $\boldsymbol{u}$, p and $\boldsymbol{s}$ and where $(\cdot,\cdot)$ is used to denote the standard $L^2(\Omega)$ inner product, without difference if scalar, vectorial or tensorial functions are concerned, but of course the second and third cases involve dot-products and contracted products respectively.

The computational domain Ω, assumed to be two dimensional for the sake of simplicity, is partitioned into a geometrically conforming decomposition

$$\bar{\Omega} = \cup_{k=1}^{K} \bar{\Omega}^k$$

$$\Omega^k \cap \Omega^l = \emptyset\ ,\ \forall k, l, k \neq l.$$

The velocity space $\boldsymbol{X}_N = X_N \times X_N$ and pressure space M_N consist of,

$$X_N = P_{N,K}(\Omega) \cap H_0^1(\Omega)\ ,\quad M_N = P_{N-2,K}(\Omega) \cap L_0^2(\Omega)$$

with standard notations for the Hilbert spaces $H_0^1(\Omega)$ and $L_0^2(\Omega)$, see e.g. [1], and with:

$$P_{N,K}(\Omega) = \{v \in L^2(\Omega); v|_{\Omega^k} \circ \boldsymbol{f}^k \in P_N(\Lambda^2), 1 \leq k \leq K\}$$

where $\boldsymbol{f}^k$ is the transformation function from the reference domain Λ^2, with $\Lambda = (-1, 1)$, to Ω^k and P_N the space of the polynomials of maximum degree N in each variable. For the reason of simplicity again, homogeneous boundary conditions have been assumed through the use of the $H_0^1(\Omega)$ space.

The term involving the material derivative, $(D_t \boldsymbol{u}_N, \boldsymbol{v}_N)$, can be handled in different ways. Thus, an implicit treatment of the time-derivative together with an explicit treatment of the advection term yields the so-called "Generalized Stokes problem" for the fully discrete version of problem (2). Here our goal is not to investigate these different ways, but to develop a stabilized spectral element formulation of problem (2), basically by using the spectral vanishing viscosity method.

2.1 The Spectral Vanishing Viscosity method

For the 1D non-linear conservation law of the scalar quantity $u(X, t)$:

$$\partial_t u + \partial_X(F(u)) = 0 \quad in\, \Lambda \times R^+,$$

where $F(u)$ is a scalar function of u (e.g. $F(u) = u^2/2$), the SVV method consists in solving:

$$\partial_t u_N + \partial_X I_N(F(u_N)) = \epsilon_N \partial_X(Q(\partial_X u_N)) \tag{3}$$

where $u_N \in P_N(\Lambda)$ and with $\epsilon_N = O(1/N)$, where I_N denotes the polynomial interpolation onto P_N and Q the spectral viscosity operator such that, with L_i for the Legendre polynomial of degree i:

$$Q\phi \equiv \sum_{i=0}^{N} \hat{Q}_i \hat{\phi}_i L_i, \quad \forall \phi, \quad \phi = \sum_{i=0}^{\infty} \hat{\phi}_i L_i$$

with: $\hat{Q}_i = 0$ if $i \leq m_N$ and $1 \geq \hat{Q}_i \geq 0$ if $i > m_N$. Typical choices for m_N are $m_N = O(\sqrt{N})$ [13] or $m_N = N/2$ [10], whereas for the Bürgers equation theoretical studies rather yield $m_N < O(N^{1/4})$ [13]. For $m_N < i \leq N$ the numerical experiments show that a smooth variation for $\hat{Q}_i$ yields better results. Thus, as in [13] we will use:

$$\hat{Q}_i = \exp\left(-\left(\frac{N-i}{m_N - i}\right)^2\right) \quad , i > m_N.$$

With $v_N \in P_N(\Lambda)$, the weak formulation of the SVV term $-\epsilon_N \partial_X(Q(\partial_X u_N))$ reads:

$$V_N = \epsilon_N (Q(\partial_X u_N), \partial_X v_N)_{L^2(\Lambda)}.$$

Let us remark that the SVV term may be made symmetric:

$$V_N = \epsilon_N (Q^{1/2}(\partial_X u_N), Q^{1/2}(\partial_X v_N))_{L^2(\Lambda)}$$

with the following definition of $Q^{1/2}$:

$$Q^{1/2}\phi \equiv \sum_{i=0}^{N} \sqrt{\hat{Q}_i}\hat{\phi}_i L_i, \quad \forall \phi, \quad \phi = \sum_{i=0}^{\infty} \hat{\phi}_i L_i$$

Indeed:

$$\begin{aligned}
V_N &= \epsilon_N \int_{-1}^{1} Q(\partial_X u_N)\partial_X v_N dX \\
&= \epsilon_N \int_{-1}^{1} \left[\sum_{i=0}^{N} \hat{Q}_i (\widehat{\partial_X u_N})_i L_i(X) \sum_{i=0}^{N} (\widehat{\partial_X v_N})_i L_i(X) \right] dX \\
&= \epsilon_N \sum_{i=0}^{N} \hat{Q}_i (\widehat{\partial_X u_N})_i (\widehat{\partial_X v_N})_i ||L_i||^2 \\
&= \epsilon_N \int_{-1}^{1} \left[\sum_{i=0}^{N} \sqrt{\hat{Q}_i} (\widehat{\partial_X u_N})_i L_i(X) \sum_{i=0}^{N} \sqrt{\hat{Q}_i} (\widehat{\partial_X v_N})_i L_i(X) \right] dX,
\end{aligned}$$

where we have used $||\cdot||$ to denote the $L^2(\Lambda)$ norm.

2.2 Preliminaries

In order to implement the SVV method in the spectral element approximation, the two following points must first be fixed:

- formulation of the SVV method when coordinate transforms are considered,

- formulation of the SVV method in the context of a multidimensional problem.

Up to our knowledge these points were generally overlooked. Thus, some details were given in [9], where systems of conservation laws were considered. However, the computational domains were in this paper rectangular, so that the problem of coordinate transforms was not really addressed. A similar remark is also relevant for our previous works, see e.g. [15], where

the geometry was 3D cartesian. In [10], it seems that a tensor product was simply used to define the spectral viscosity operator (see eq. (11) of [10]) and no more details were given. It should be noticed that the tensor product implementation of the SVV method differs from what was utilized in [9]. From our point of view, the proper implementation of the SVV method in a spectral element approximation requires to go into some "technical details", which moreover are not specific to the Navier-Stokes equations.

Let us consider a coordinate transform, say $x = f(X)$ with $x \in \Omega$ and $X \in \Lambda$, and give a meaning to the SVV term:

$$V_N = \epsilon_N (Q(\partial_x u_N), \partial_x v_N)_{L^2(\Omega)}$$

where the ϵ_N value may differ from the one used with the reference domain. Of course, we have first to express $\partial_x u_N$ as a function of $X \in \Lambda$:

$$\partial_x u_N(x) = \widetilde{\partial_x g}(X)\, \partial_X \tilde{u}_N(X)$$

where g is the inverse of f, $X = g(x)$ and $\tilde{\varphi} = \varphi \circ f$. From the above form it is possible to compute $Q(\partial_x u_N)$. However such an approach is to be rejected, because the goal is in fact to damp the high frequency range of $\tilde{u}_N \in P_N(\Lambda)$. Thus, in another context of the spectral element method, if the coordinate transform was used to accumulate some grid-points in a region of strong variation of the exact solution, then possibly it would be unnecessary to smooth its numerical approximation u_N through the use of a dissipation term. This is why we state that:

$$Q(\partial_x u_N) \equiv \widetilde{\partial_x g} \sum_{i=0}^{N} \hat{Q}_i (\widehat{\partial_X \tilde{u}_N})_i L_i.$$

When expressed in the reference domain Λ, the SVV term reads:

$$\begin{aligned} V_N &= \epsilon_N (\widetilde{\partial_x g}\, Q(\partial_X \tilde{u}_N), \partial_X f\, \widetilde{\partial_x g}\, \partial_X \tilde{v}_N)_{L^2(\Lambda)} \\ &= \epsilon_N (\widetilde{\partial_x g}\, Q(\partial_X \tilde{u}_N), \partial_X \tilde{v}_N)_{L^2(\Lambda)}. \end{aligned} \tag{4}$$

Such a term can only be made symmetric if $\partial_x g$ is constant, i.e. if g (equivalently f) is a linear mapping. In this case, (4) can be written:

$$V_N = \epsilon_N\, (\partial_X f)^{-1} (Q^{1/2}(\partial_X \tilde{u}_N), Q^{1/2}(\partial_X \tilde{v}_N))_{L^2(\Lambda)}$$

where, in order to conform with the definition in (3), ϵ_N should be chosen such that:

$$\epsilon_N\, (\partial_X f)^{-1} = O(\frac{1}{N}).$$

that is:

$$\epsilon_N = O(\frac{L_x}{2N}).$$

where L_x is the length of Ω.

In the frame of the spectral element implementation, it is highly desirable to handle in any case a symmetric form. To this end we come back to the case where f is not a linear mapping and introduce the symmetric bilinear form:

$$V_N^s = \epsilon_N(\widetilde{\partial_x g}\, Q^{1/2}(\partial_X \tilde{u}_N), Q^{1/2}(\partial_X \tilde{v}_N))_{L^2(\Lambda)} \tag{5}$$

where we may suppose that $\widetilde{\partial_x g} > 0$.

It is clear that the above expression may be written as a weighted inner product:

$$V_N^s = \epsilon_N(Q^{1/2}(\partial_X \tilde{u}_N), Q^{1/2}(\partial_X \tilde{v}_N))_{L^2_\mu(\Lambda)}$$

where $\mu = \widetilde{\partial_x g}$ stands for the weight function. As a result of the equivalence between the $L^2(\Lambda)$ and $L^2_\mu(\Lambda)$ norms ($+\infty > \mu > 0$), $V_N^s(\tilde{u}_N, \tilde{u}_N) \sim V_N(\tilde{u}_N, \tilde{u}_N) > 0$, if $\tilde{u}_N \neq 0$. Consequently V_N^s constitutes a SVV term, in the sense that it is dissipative and, as V_N, controlled by the the parameters m_N and ϵ_N. Of course, its expression is coherent with the result obtained within the linear mapping assumption for which $\mu = \partial_x g = (\partial_X f)^{-1}$ is constant.

Let us go now to the multidimensional case, e.g. to the 2D case which can easily be generalized to the 3D one. With $u_N, v_N \in P_N(\Lambda^2)$ the 1D formulation extends in:

$$V_N = \epsilon_N(Q(\nabla u_N), \nabla v_N)_{L^2(\Lambda^2)}$$

where, for the sake of simplicity, we have kept the same notation for the operator Q acting on vector functions and scalar functions. However the meaning of $Q(\nabla u_N)$ must be clarified; From the 1D scalar definition of Q we define $Q(\nabla u_N)$ as follows:

$$Q(\nabla u_N) \equiv \begin{pmatrix} Q^1(\partial_X u_N) \\ Q^2(\partial_Y u_N) \end{pmatrix} \tag{6}$$

where

$$Q^1(\partial_X u_N) \equiv Q(\partial_X u_N(\cdot, Y)) = \sum_{i=0}^{N} \hat{Q}_i(\widehat{\partial_X u_N})_i(Y) L_i(X)$$

$$Q^2(\partial_Y u_N) \equiv Q(\partial_Y u_N(X, \cdot)) = \sum_{i=0}^{N} \hat{Q}_i(\widehat{\partial_Y u_N})_i(X) L_i(Y)$$

so that dissipative terms arise in both X and Y directions, as desired. Moreover, one may easily check that V_N can still be made symmetric:

$$V_N = \epsilon_N(Q^{1/2}(\nabla u_N), Q^{1/2}(\nabla v_N))_{L^2(\Lambda^2)}.$$

Although some details are missing in [9], it seems that the 2D extension of the initial 1D SVV method proposed in this paper was similar to ours. However it was a collocation method which was finally used in [9], so that no symmetrization was carried out.

At this point it is of interest to emphasize that the above definition of Q may be discussed. Thus, using the 2D Legendre polynomial basis, in Λ^2 one may think to define an operator Q such that:

$$Q\boldsymbol{\phi} \equiv \sum_{i=0}^{N}\sum_{j=0}^{N} \hat{Q}_{ij}\boldsymbol{\phi}_{ij}L_iL_j, \quad \forall \boldsymbol{\phi}, \quad \boldsymbol{\phi}(X,Y) = \sum_{i=0}^{\infty}\sum_{j=0}^{\infty} \boldsymbol{\phi}_{ij}L_i(X)L_j(Y)$$

and the problem is then to provide the $\hat{Q}_{ij}$. To this end, it is natural to restart from the 1D definition. However, the tensor product $\hat{Q}_{ij} = \hat{Q}_i\hat{Q}_j$ must be rejected, because the SVV term would then be only active if $i > m_N$ and $j > m_N$. To see that readily, the SVV term may be detailed, in strong formulation, into:

$$\nabla \cdot Q(\nabla u_N) = \sum_{i,j=0}^{N} \hat{Q}_i\hat{Q}_j((\widehat{\partial_X u_N})_{ij}L_i'(X)L_j(Y) + (\widehat{\partial_Y u_N})_{ij}L_i(X)L_j'(Y))$$

where $'$ is used to denote the differentiation. Taking an extreme case where the solution u_N depends only on X, i.e. $u_N \equiv u_N(X)$, then $(\widehat{\partial_X u_N})_{ij} = 0$ if $j \neq 0$, which means that no spectral viscosity acts even in X direction. This remains true if $(\widehat{u_N})_{ij} = 0$ for $j > m_N$.

One may consider a definition such that the SVV term acts if $i > m_N$ or $j > m_N$. This can be achieved for instance by assuming:

$$\hat{Q}_{ij} = 1 - (1 - \hat{Q}_i)(1 - \hat{Q}_j) = \hat{Q}_i + \hat{Q}_j - \hat{Q}_i\hat{Q}_j.$$

However in this case the SVV term reads:

$$\nabla \cdot Q(\nabla u_N) =$$
$$\sum_{i,j=0}^{N} (\hat{Q}_i + \hat{Q}_j - \hat{Q}_i\hat{Q}_j)((\widehat{\partial_X u_N})_{ij}L_i'(X)L_j(Y) + (\widehat{\partial_Y u_N})_{ij}L_i(X)L_j'(Y)),$$

which may induce a non-desired dissipative term. For example, if u_N does not show high frequencies in the Y direction, i.e. $(\widehat{u_N})_{ij} = 0$ if $j > m_N$, we

obtain:

$$\nabla \cdot Q(\nabla u_N) = \sum_{i,j=0}^{N} \hat{Q}_i((\widehat{\partial_X u_N})_{ij} L_i'(X) L_j(Y) + (\widehat{\partial_Y u_N})_{ij} L_i(X) L_j'(Y))$$

where the second term in the right hand side should be rejected.

On the contrary with the definition (6) we obtain:

$$\nabla \cdot Q(\nabla u_N) = \sum_{i=0}^{N} \hat{Q}_i(\widehat{\partial_X u_N})_i(Y) L_i'(X) + \sum_{j=0}^{N} \hat{Q}_j(\widehat{\partial_Y u_N})_j(X) L_j'(Y)$$

so that if u_N does not show high frequencies in Y direction:

$$\nabla \cdot Q(\nabla u_N) = \sum_{i=0}^{N} \hat{Q}_i(\widehat{\partial_X u_N})_i(Y) L_i'(X).$$

To conclude this Section, let us consider the case of vector functions. With $\boldsymbol{u}_N = (u_1, u_2)$, the coherent extension of our previous definition for scalar functions reads:

$$Q(\nabla \boldsymbol{u}_N) \equiv \begin{pmatrix} Q^1(\partial_X u_1) & Q^2(\partial_Y u_1) \\ Q^1(\partial_X u_2) & Q^2(\partial_Y u_2) \end{pmatrix} \tag{7}$$

2.3 Spectral element implementation

Let $\boldsymbol{f}$ be the mapping from (X, Y), in the reference element Λ^2, to (x, y) in the element Ω^k and $\boldsymbol{g} = \boldsymbol{f}^{-1}$, G the Jacobian matrix of $\boldsymbol{g}$ and J the Jacobian determinant of $\boldsymbol{f}$ (for the sake of simplicity in the notation we use $\boldsymbol{f}$, $\boldsymbol{g}$, ..., rather than $\boldsymbol{f}^k$, $\boldsymbol{g}^k$, ...). As a result of our previous investigations, the SVV term reads:

$$V_N = \epsilon_N (Q(\tilde{\nabla} \tilde{\boldsymbol{u}}_N) \tilde{G}, (\tilde{\nabla} \tilde{\boldsymbol{v}}_N) \tilde{G} J)_{L^2(\Lambda^2)} \tag{8}$$

where $\tilde{\nabla}$ denotes the gradient with respect to the reference domain and with $\tilde{\varphi} = \varphi \circ \boldsymbol{f}$.

This form can only be made symmetric if G is constant and diagonal. Note that if G is constant but non-diagonal then cross terms arise in the above L^2 product, e.g.:

$$\int_{\Lambda^2} (\tilde{G}_{11} \sum_{i=0}^{N} \hat{Q}_i(\widehat{\partial_X \tilde{u}_1})_i(Y) L_i(X))(J \tilde{G}_{21} \sum_{j=0}^{N} (\widehat{\partial_Y \tilde{v}_1})_j(X) L_j(Y)) dX dY \neq 0$$

where we have used again the notation $\boldsymbol{u}_N = (u_1, u_2)$. If G is constant and diagonal, that is if the element is a rectangle, then:

$$V_N = \epsilon_N \, J(Q^{1/2}(\tilde{\nabla}\tilde{\boldsymbol{u}}_N)\tilde{G}, Q^{1/2}(\tilde{\nabla}\tilde{\boldsymbol{v}}_N)\tilde{G})_{L^2(\Lambda^2)}.$$

Just like in 1D it is of interest to provide a symmetric SVV term valid for any mapping $\boldsymbol{f}$. To this end we introduce the symmetric bilinear form:

$$V_N^s = \epsilon_N (Q^{1/2}(\tilde{\nabla}\tilde{\boldsymbol{u}}_N)\tilde{G}, Q^{1/2}(\tilde{\nabla}\tilde{\boldsymbol{v}}_N)\tilde{G}J)_{L^2(\Lambda^2)} \tag{9}$$

where we may suppose (without loss of generality) that $J > 0$. With tr for trace, ":" to denote the contracted product and exponent t to denote the transposition, one has:

$$(Q^{1/2}(\tilde{\nabla}\tilde{\boldsymbol{u}}_N)\tilde{G}) : (Q^{1/2}(\tilde{\nabla}\tilde{\boldsymbol{v}}_N)\tilde{G}J) = tr(Q^{1/2}(\tilde{\nabla}\tilde{\boldsymbol{u}}_N)\tilde{G}JG^t(Q^{1/2}(\tilde{\nabla}\tilde{\boldsymbol{v}}_N))^t)$$

so that V_N^s may be expressed as the sum of inner products of vector valued functions involving the symmetric positive definite weight matrix $\mu = \tilde{G}J\tilde{G}^t$:

$$V_N^s = \epsilon_N[(Q^{1/2}(\tilde{\nabla}\tilde{u}_1), Q^{1/2}(\tilde{\nabla}\tilde{v}_1))_{L^2_\mu(\Lambda^2)} + (Q^{1/2}(\tilde{\nabla}\tilde{u}_2), Q^{1/2}(\tilde{\nabla}\tilde{v}_2))_{L^2_\mu(\Lambda^2)}].$$

Then, as in the 1D case, V_N^s, as defined in (9), constitutes a SVV term.

Coming back to the Navier-Stokes system, we obtain the following semi-discrete problem: Find $\boldsymbol{u}_N \in \boldsymbol{X}_N$ and $p_N \in M_N$ such that

$$\left\{ \begin{array}{rl} (D_t\boldsymbol{u}_N, \boldsymbol{v}_N) + \nu(\nabla\boldsymbol{u}_N, \nabla\boldsymbol{v}_N) - & \\ (\nabla\cdot\boldsymbol{v}_N, p_N) + \epsilon_N(Q^{1/2}(\nabla\boldsymbol{u}_N), Q^{1/2}(\nabla\boldsymbol{v}_N)) & = (\boldsymbol{s}_N, \boldsymbol{v}_N) \ , \ \forall \boldsymbol{v}_N \in \boldsymbol{X}_N \\ (\nabla\cdot\boldsymbol{u}_N, q_N) & = 0 \ , \ \forall q_N \in M_N \end{array} \right. \tag{10}$$

where a clear sense has been given to the SVV term. Note that as in 1D, ϵ_N must take into account a characteristic length of the elements. With h such a dimensionless length: $\epsilon_N = O(h/2N)$.

Problem (10) can be handled as it stands by SEM. However, for the sake of numerical efficiency, it would be of interest to couple the computation of the viscous and SVV terms. To this end let us add the viscous term of the Navier-Stokes equations and the non-symmetric SVV term (8) to obtain:

$$\nu(\nabla\boldsymbol{u}_N, \nabla\boldsymbol{v}_N)_{L^2(\Omega^k)} + V_N = \nu(S(\tilde{\nabla}\tilde{\boldsymbol{u}}_N)\tilde{G}, \tilde{\nabla}\tilde{\boldsymbol{v}}_N\tilde{G}J)_{L^2(\Lambda^2)}$$

where S stands for:

$$S = I + \frac{\epsilon_N}{\nu}Q$$

with I for the identity operator.

Then, following an approach similar to the one we have just described, we can introduce the "viscous stabilizing term", say T_N such that:

$$T_N = \nu(S^{1/2}(\tilde{\nabla}\tilde{\boldsymbol{u}}_N)\tilde{G}, S^{1/2}(\tilde{\nabla}\tilde{\boldsymbol{v}}_N)\tilde{G}J)_{L^2(\Lambda^2)}. \tag{11}$$

The spectral element approximation is usually based on a nodal basis. Then this form is easy to implement, since after discretization one has simply to substitute the Legendre differentiation matrix, say D, by the matrix $S^{1/2}D$, where $S^{1/2}$ reads:

$$S^{1/2} = M^{-1} diag(1 + \frac{\epsilon_N}{\nu}\hat{Q}_i)^{1/2} M$$

with M: passage matrix from physical space to spectral Legendre space. As a result, using such a "viscous stabilizing term" allows us to stabilize the scheme without additional computational time per iteration (resp. time-step) if an iterative (resp. direct) solver is used for the final system of algebraic equations.

The stabilized spectral element formulation of the semi-discrete Navier-Stokes system then writes:

$$\begin{cases} (D_t\boldsymbol{u}_N, \boldsymbol{v}_N) + \nu(S^{1/2}(\nabla\boldsymbol{u}_N), S^{1/2}(\nabla\boldsymbol{v}_N)) - \\ \qquad\qquad (\nabla\cdot\boldsymbol{v}_N, p_N) &= (\boldsymbol{s}_N, \boldsymbol{v}_N)\ ,\ \forall \boldsymbol{v}_N \in \boldsymbol{X}_N \\ \qquad\qquad (\nabla\cdot\boldsymbol{u}_N, q_N) &= 0\ ,\ \forall q_N \in M_N \end{cases} \tag{12}$$

Of course, the usual viscous term is recovered as soon as $\epsilon_N = 0$ or $m_N = N$, and if the mappings from Λ^2 to the Ω^k are linear and diagonal, then the proposed formulation is equivalent to the previous (symmetric or non-symmetric) ones.

Details on the practical implementation of the viscous term T_N are provided in Appendix.

3 Accuracy tests

In this Section we focus on:

- an elliptic Helmholtz equation, solved by a steep analytical solution, to demonstrate that the stabilized spectral element approximation retains the exponential accuracy. We begin with the Fourier approximation of the standard 1D periodic case and proceed with a 2D problem which we handle with spectral elements.

- the so-called "Kovasznay flow", which constitutes an exact solution of the incompressible Navier-Stokes equations.

3.1 Elliptic Helmholtz problem

3.1.1 1D Fourier test

The basic idea is to consider an exact solution of the form: $u = \tanh(\alpha x)$ in $(-1, 1)$. However, tests are made with the following modified exact solution: $u = \exp(-10x^2)\tanh(\alpha x)$ in order to recover (at least approximatively) the periodicity. In all our tests $\alpha = 50$.

Using such an analytical solution we can set up the source term of the following Helmholtz-like equation:

$$-\nu\partial_x^2 u + u = s, \quad \nu \geq 0.$$

Two values of ν have been considered: $\nu = 0$ and $\nu = 1/\alpha^2$.

Concerning the SVV parameters, we have used the following values of ϵ_N and m_N:

- $\epsilon_N = 1/N$ and $\epsilon_N = 1/2N$,
- $m_N = \sqrt{N}$ and $m_N = N/2$,

where here N is the maximal wavenumber.

In Fig.1 we present some accuracy results in both L^2 and H^1 norms. Clearly, the errors show an exponential decay, since in this semi-log representation one observes that the error variations are essentially linear versus the number of grid-points. The dependence of the results with respect to ν appears to be rather weak. On the contrary, the influence of the characteristic parameters of the SVV method is more important. Thus, as could be expected, the convergence rate is better when decreasing the value of ϵ_N or when increasing the value of m_N.

3.1.2 2D spectral element test

Here we consider the 2D analogue of the previous 1D test case:

$$\begin{aligned} &-\nu\nabla^2 u + u = s \quad in\, \Omega = (-1, 1)^2 \\ &u|_\Gamma = u_\Gamma \end{aligned}$$

in order to check numerically its SVV-stabilized spectral element formulation: Find $u_N \in X_N$, such that

$$(u_N, v_N) + \nu(S^{1/2}(\nabla u_N), S^{1/2}(\nabla v_N)) = (s_N, v_N)\ ,\ \forall v_N \in X_N. \tag{13}$$

For the exact solution we choose the analytical function:

$$u(x, y) = \tanh(\alpha\frac{\sqrt{2}}{2}(x - y))\tanh(\alpha\frac{\sqrt{2}}{2}(x + y)) \tag{14}$$

with $\alpha = 50$ as in the 1D test. Fig.2 shows the sharp form of this solution.

The computational domain is first partitioned in 10×10 square elements and we successively study (i) the influence of the SVV stabilization technique on the accuracy of the SEM solution, (ii) the sensitivity of the error to the viscosity parameter ν and (iii) the dependence of the error on the characteristic parameters m_N and ϵ_N of the SVV stabilization.

Second, we consider a deformed mesh and point out that a mesh deformation does not deteriorate the accuracy properties of the SVV spectral element approximation.

Fig.3 shows some accuracy results (in H^1, L^2 and L^∞ norms) obtained with the stabilized and the non-stabilized formulations. Here the SVV method is used with $m_N = N/2$ and $\epsilon_N = 1/N$. As expected from the 1D results, even though the SVV-SEM is less accurate than the SEM, the errors show an exponential decay when the polynomial degree is increased.

In Fig.4 it is the influence of the viscosity ν which is pointed out. Here again, $m_N = N/2$ and $\epsilon_N = 1/N$. Essentially, as for the 1D tests one observes that the results depend only weakly on the value of ν: similar errors are obtained with $\nu = 10^{-2}$ and $\nu = 10^{-4}$.

In Fig.5 we study the influence of the spectral viscosity activation parameter m_N. The convergence results have been obtained for the following values of m_N: $\sqrt{N}$, $N/2$, $2N/3$ and $N-2$. The value of ϵ_N is $\epsilon_N = 1/N$. Clearly the best results are obtained for m_N close to N.

Fig.6 shows the sensitivity of the error to the viscosity parameter amplitude ϵ_N. The value of m_N is fixed to $m_N = N/2$ and results obtained with $\epsilon_N = 1/N$ and $\epsilon_N = 0.1/N$ are compared. Note that this last value is coherent with the theoretical analysis, from which $\epsilon_N = O(h/2N)$. It appears that only slightly better results are obtained with the lower value of ϵ_N, with a negligible difference in the convergence rate. Clearly, changing m_N is here much more significant than changing ϵ_N. The fact that only low values of N are used in the spectral element approximation may provide an explanation for this weak dependence of the error on the ϵ_N value.

Let us now point out the influence of a deformation of the mesh. This is especially important as pointed out in the theoretical part: If the mappings from the reference domain $(-1,1)^2$ to the spectral elements are linear and diagonal then the different approaches described in Section 2 are equivalent. The deformed spectral element mesh is shown in Fig.7. Here using a non-symmetric SVV term, a symmetrized one or the stabilized viscous term is no longer equivalent.

Fig.8 compares the results obtained with the deformed mesh and with the regular one. Here we have used $m_N = 2N/3$ and $\epsilon_N = 1/N$. One observes that the errors still decrease exponentially as N increases, which means that

the stabilized formulation remains spectrally accurate. Moreover, we note that the convergence rate is roughly the same for the two considered meshes, i.e. with and without mesh deformation.

The main conclusions of the study carried out in this Section for the elliptic Helmholtz equation are the following:

- Although less accurate than the SEM, the SVV-SEM remains spectrally accurate,

- Using a deformed mesh preserves the exponential convergence property.

3.2 Kovasznay flow

The following velocity and pressure fields

$$\boldsymbol{u} = (1 - \exp(\lambda x)\cos(2\pi y), \frac{\lambda}{2\pi}\exp(\lambda x)\sin(2\pi y)) \quad and \quad p = -\frac{1}{2}\exp(2\lambda x)$$

where $\lambda = Re/2 - (Re^2/4 + 4\pi^2)^{0.5}$, exactly solve the incompressible Navier-Stokes equations. Just like for the elliptic Helmholtz problem, it is then of interest to check the influence of the spectral vanishing viscosity term on the accuracy of the spectral element solution.

Tests have been carried out in the domain $\Omega = (-0.5, 1)\times(-0.5, 1.5)$, with the spectral element mesh shown in Fig. 9, for $Re = 40$ and using Dirichlet boundary conditions. Such a test was considered in [10], where it appeared that the SVV method retains the accuracy of the spectral approximation, on the contrary of what we have obtained for the elliptic Helmholtz problem.

Our results are presented in Fig. 10, where we show the errors $||\boldsymbol{u}-\boldsymbol{u}_{exact}||$ in different norms for $m_N = N - 2$ and $m_N = N/2$. Clearly, for $m_N = N - 2$, the results obtained with SVV are slightly better than those obtained without. Thus, although the Navier-Stokes solver is based on an elliptic solver (see next Section) yielding worse results when the SVV is activated, this Navier-Stokes solver may yield better results with SVV than without! Moreover, a similar result has been recently obtained for a time-dependent analytical solution by one of the authors [24]. The non-linear term may be responsible for such a behavior: Especially, one may think that the spurious "high-frequency modes" resulting from aliasing effects are damped when the SVV is activated. Nevertheless, for $m_N = N/2$, one recovers the expected behavior, with a better accuracy when the SVV is not activated, and also slight differences in the convergence rates.

From our point of view the fact that the Kovasznay exact solution is very smooth is misleading. For the Helmholtz problem, close results can also be obtained with or without SVV, if the solution is too smooth. Beyond a critical wavenumber, the "exact solution" (within the computational accuracy) is

captured, so that nothing changes if m_N is chosen greater than this value. Concerning the results reported in [10], we think that their implementation of the SVV method together with the fact that the Kovasznay exact solution is much smoother in x-direction than in y-direction may explain why it was found that the spectral accuracy was retained (cf. Section 2.2). In any cases, at this point of the discussion more numerical experiments are required before going to a conclusion.

In the next Section the stabilization capabilities of the proposed SVV stabilized spectral element formulation are demonstrated through the computation of the 2D high Reynolds number wake of a cylinder.

4 Flow past a cylinder

The $P_N \times P_{N-2}$ spectral element approximation of the Navier-Stokes system, as briefly described in Section 2, has been largely used in numerical simulations of incompressible flows in the two last decades. However, for the reasons mentioned in Introduction, it is also known that stability problems have been encountered in the use of SEM for the computation of high Reynolds number flows, especially transitional laminar-turbulent flows.

To show the efficiency of the proposed SVV stabilized SEM, several calculations have been carried out for the flow around an impulsively started circular cylinder, the Reynolds number being varied from $Re = 300$ up to $Re = 1000$. Such 2D flows are of course not physical, since the 2D-3D transition occurs for $Re \approx 190$, but our goal here is only to check the capabilities of the SVV-SEM in a case where the standard SEM would not converge for reasonable time and space discretizations.

The temporal discretization is based upon an operator splitting approach in which the nonlinear convective term is decoupled from the viscous and divergence operators via an operation-integration-factor technique introduced in [12] and studied e.g. in [4, 23]. This temporal discretization results in a saddle point problem coupling the velocity and the pressure, which is decoupled later via an additional splitting step. Such an algorithm was analyzed and applied to various computations in [18, 4, 5]. The approach has a common root with traditional projection approaches which lead to a Poisson equation for the pressure except that, in the present case, the splitting is done for the discrete form of the equations, and therefore no boundary conditions are needed for the pressure.

Dirichlet boundary conditions, i.e. $\boldsymbol{u}_N = (1, 0)$, have been assumed everywhere except at the outlet of the computational domain where "Orlanski's outflow boundary conditions", $\partial_t \boldsymbol{u} + U_\infty \cdot \nabla \boldsymbol{u} = 0$, have been imposed, where

U_∞ is the free stream velocity (see e.g. [22] for details). At time $t = 0$ the fluid is at rest, i.e. the initial condition simply reads $\boldsymbol{u}_N = 0$.

Fig.11 shows the macro-element mesh used in the calculations. Finer elements have been chosen at the cylinder surface for a better resolution of the boundary layer. In all our calculations, the number of the elements has been fixed to $K = 310$. Mesh notation Nx means using polynomial degree x in each element.The Reynolds number is defined as $Re = U_\infty D/\nu$, where D is the cylinder diameter. In this domain decomposition, using the standard SEM we were unable to compute flows at $Re \geq 500$ at any reasonable resolution. For example,

- at Re=500: The *N6* computation diverges at $t = 5.9$, *N10* diverges at $t = 15.9$ and *N12* diverges at $t = 16.4$;

- at $Re = 1000$: *N6* diverges at $t = 1.9$, *N12* diverges at $t = 9.84$ and *N16* diverges at $t = 11.01$ (moreover, this last computation was very costly).

By contrast, using the SVV-stabilized formulation with $m_N = 2N/3$ and $\epsilon_N = 1/N$ for example, we were able to compute all these flows for all the above mentioned polynomial approximations. Hereafter we study the influence of the parameters N, m_N and ϵ_N, by focusing on a sensitive computational result: the vorticity variations at the cylinder surface during the development of the wake. Such vorticity variations are particularly of interest, to be sure that the use of a "viscous stabilizing term" would not deteriorate the numerical results in those regions of the flow dominated by viscous effects, especially the boundary layer around the cylinder.

4.1 Influence of the polynomial approximation degree

Here we check the spatial resolution, i.e. the sensitivity of the results to an increase of the polynomial approximation degree. Several values of the polynomial degree have been used in the calculation at $Re = 1000$. In this space discretization study, the SVV parameters have been fixed to $m_N = 2N/3$ and $\epsilon_N = 1/N$.

In Fig.12, we compare the vorticity distribution at the cylinder surface calculated, at time $t = 6$, with different values of N. Also shown is a result given in [19] for comparison. For $N = 6$, the resolution seems to be inaccurate, but already comparable with the one of [19]. However the convergence is obvious by increasing N: For N varying from $N = 8$ to 16 the results are very close, indicating that for $N \geq 8$ the grids are fine enough to capture all the flow structures.

The vorticity isolines at $t = 4$ and $t = 6$ are shown in Fig.13 for the cases *N6*, *N8* and *N12*. Clearly, the *N6* grid is not fine enough to give smooth

vorticity contours. For *N8* and *N12*, although one observes slight differences close to the cylinder surface, the vorticity fields compare well.

4.2 Influence of the SVV tuning parameters

Here we check the effect of the parameters ϵ_N and m_N on the computational results, with comparison to the "reference result" obtained with the very fine grid *N16*, the SVV parameters being $m_N = N - 2$ and $\epsilon_N = 1/N$.

Fig.14 shows the vorticity variations at the cylinder surface, at $t = 6$, computed with $\epsilon_N = 1/N$ and $\epsilon_N = h/2N$, m_N being fixed to $m_N = 2N/3$, where $h = 1/7.2$ equals the ratio of the cylinder diameter to the domain height. These variations are compared to the reference ones. One observes, for $N = 6$ and $N = 9$ on the figure, that the choice $\epsilon_N = h/2N$ gives better results. When increasing the value of N, the curves get closer to the reference one. Thus, for $N = 12$ (not shown), one can no longer discern the three curves.

In Fig.15, where again $N = 6$ and $N = 9$, the vorticity distribution at the cylinder surface is plotted for $m_N = N/3$ and $m_N = N - 2$, with $\epsilon_N = 1/N$. A better result is obtained by using a higher value of m_N, i.e., $m_N = N - 2$. This difference is in fact less significant when a smaller ϵ_N (i.e. $\epsilon_N = h/2N$) is used. For larger values of m_N and/or smaller values of ϵ_N, it is still possible to get a SVV stabilization effect. However, for the considered test-case we have checked that the value $m_N = N - 2$ was the maximal one: For $m_N = N - 1$, the calculations were not stable.

Better results are thus obtained when decreasing the amplitude ϵ_N or when increasing the SVV activation parameter m_N. However it is remarkable that even for a large values of m_N the SVV stabilization can still remain efficient. The value $m_N = N - 2$ is indeed much greater than what could be expected from the theoretical studies carried out for the Bürgers equation.

4.3 Long time behavior

The stabilization effect of the SVV term is furthermore confirmed by the long time simulation of the unsteady wake at $Re = 1000$. The *N12* mesh is used for the simulation and the time step equals 0.02, using 5 sub time-cycles in the transport step. No artificial perturbation was applied to the flow to initiate the vortex shedding. The SVV parameters used in the computation are $\epsilon_N = 1/N$ and $m_N = N - 2$. Fig.16 shows the vorticity isolines at time $t = 160, 162$, i.e. approximatively on a half-period, to clearly visualize the well-known vortex shedding phenomenon. The corresponding streamlines are shown in Fig.17. From the time evolution of the cross-flow velocity we obtain

a Strouhal number (dimensionless frequency) of 0.251. This result is in good agreement, although slightly higher, with those of [19] and the references therein (see Table I of [19]).

Let us conclude this Section as follows: the SVV stabilized SEM allows us to compute flows out of reach of the standard SEM and the best accuracy is obtained for the highest values of m_N and the smallest of ϵ_N. As a result, for a particular mesh, we should take ϵ_N minimal and m_N maximal whenever the calculation is stable. For a given problem and computational mesh, there exist of course critical values of ϵ_N and m_N beyond which the SVV-SEM is no longer stable. Thus, the computation with $\epsilon_N = h/2N$ and $m_N = N - 1$ is not stable, but ($\epsilon_N = h/2N$, $m_N = 2N/3$) and ($\epsilon_N = 1/N$, $m_N = N - 2$) are stable. Until now we do not know how to select the most satisfactory values of ϵ_N and m_N for a particular simulation. This crucial point will be further investigated in the future.

5 Concluding remarks

The highly accurate computation of high-Reynolds number flows is of real interest for both fundamental studies, e.g. concerned with the transition to turbulence, and engineering applications, which generally involve non-laminar flows. When using spectral elements the computation of such flows is a challenging task, as a result from the fact that they are much less affected than low order methods by numerical diffusion. On the grounds of the SVV method, initially introduced for 1D conservation laws, we have proposed a new approach resulting in a stabilized formulation of the SEM for the Navier-Stokes equations. It should be mentioned that this formulation yields an algorithm which can be easily implemented in any spectral element solver and which does not require additional computational time per iteration, the stabilization term being included in the viscous term.

First, a detailed study of the convergence properties of the SVV-SEM has been provided for the Helmholtz-elliptic solver. Using a steep analytical solution, it has been shown that the exponential property of the spectral method is preserved although if the convergence rate worsens. However, this may be no longer true for the Navier-Stokes equations, when a smooth analytical solution is considered: For the Kovasznay flow, we have found that with a high value of the SVV activation parameter the results could be slightly better when the SVV is activated.

Second, to demonstrate the stabilization capabilities of the SVV-SEM for the Navier-Stokes equations, we have computed the wake of a cylinder at high Reynolds number and again, the influence of the SVV parameters on

the results has been pointed out.

Beyond the computation of high Reynolds number flows, the algorithm that we propose is well adapted to the LES of turbulent flows and the interest in the SVV method for LES was e.g. outlined in [10, 15, 3]. The SVV-SEM may then be used as a no-model approach, i.e. no modeling of the sub-grid scale tensor which results from the spatial filtering of the Navier-Stokes equations. However, it can also be combined with such a modeling, then providing a way to avoid a non-controlled mixing between the modeling adjustments and the numerical approximation errors. Thus, in [15, 3] a SVV stabilization is used together with an approximate deconvolution technique [7, 20]. In the frame of 3D spectral Chebyshev-Fourier computations of the turbulent wake of a cylinder, some comparisons of the two possible routes are provided in [17], but of course, numerous detailed studies are still needed. In this frame, our goal is to apply the SVV-SEM to LES of complex turbulent flows, with or without sub-grid scale modeling, and thus provide additional contributions to the challenging topic of their highly accurate computations.

Acknowledgments

Part of this work was done when C.J. Xu was in Lab. J.A. Dieudonné as invited professor of the University of Nice-Sophia Antipolis (March-April 2003). We thank J.M. Lacroix, engineer of the CNRS, for his helpful contribution to this paper.

References

[1] Adams, R.A., Sobolev spaces, Academic Press, New-York, San Francisco, London (1975).

[2] Boyd, J.P., Two comments on filtering (artificial viscosity) for Chebyshev and Legendre spectral and spectral element methods: Preserving the boundary conditions and interpretation of the filter as a diffusion, *J. Comput. Phys.*, **143**, p.283-288 (1998).

[3] Cousin, L. and Pasquetti, R., High-order order methods for the simulation of transitional to turbulent wakes, *Proc. of the SCA 03 Conf.*, in press.

[4] Couzy, W. and Deville, M.O., A fast Schur complement method for the spectral element discretization of the incompressible Navier-Stokes equations, *J. Comput. Phys.*, **116**, p.135-142 (1995).

[5] Fischer, P., An overlapping Schwarz method for spectral element solution of the incompressible Navier-Stokes equations, *J. Comput. Phys.*, **133**, p.84-101 (1997).

[6] Fischer, P. and Mullen, J., Filter-based stabilization of spectral element methods, *C. R. Acad. Sci. Paris*, **332** (1), p.265-270 (2001).

[7] Geurt, B.J., Inverse modeling for large-eddy simulation, *Phys.Fluids*, **9**(12), p.3585-3587 (1997).

[8] Guo, B., Ma, H. and Tadmor, E., Spectral vanishing viscosity method for nonlinear conservation laws. *SIAM J. Numer. Anal.* **39**, No.4, p.1254-1268 (2001).

[9] Kaber, O.S.M., A Legendre pseudospectral viscosity method, *J. Comput. Phys.*, **128**, p.165-180 (1996).

[10] Karamanos, G.S. and Karniadakis, G.E., A spectral vanishing viscosity method for large-eddy simulation, *J. Comput. Phys.*, **163**, p.22-50 (2000).

[11] Maday, Y. and Patera, A.T., *Spectral element methods for the Navier-Stokes equations*, In A.K. Noor (ed.), State-of-the-art surveys in computational mechanics, ASME, New York, p.71-143 (1988).

[12] Maday, Y., Patera, A.T. and Ronquist, E.M., An operator-integration-factor splitting method for time-dependent problems: application to incompressible fluid flow, *J. Sci. Comp.*, **5** (4), p.263-292 (1990).

[13] Maday, Y., Kaber, S.M.O. and Tadmor, E., Legendre pseudo-spectral viscosity method for nonlinear conservation laws, *SIAM J. Numer. Anal.*, **30** (2), p.321-342 (1993).

[14] Von Neumann J. and Richtmyer R.D., A method for the calculation of hydrodynamic shocks, *J. Appl. Phys.*, **21**, p.232-237 (1950).

[15] Pasquetti, R. and Xu, C.J., High-order algorithms for large eddy simulation of incompressible flows, *J. Sci. Comp.*, **17** (1-4), p.273-284 (2002).

[16] Pasquetti, R. and Xu, C.J., Comments on "Filter-based stabilization of spectral element methods", *J. Comput. Phys.*, **182**, p.646-650 (2002).

[17] Pasquetti, R., High-order LES modeling of incompressible turbulent flows, *CRAS*, in press.

[18] Perot, J.B., An analysis of the fractional step method, *J. Comput. Phys.*, **108**, p.51-58 (1993).

[19] Qian, L. and Vezza, M., A Vorticity-based method for incompressible unsteady viscous flows, *J. Comput. Phys.* , **172**, p.515-542 (2001).

[20] Stolz, S. and Adams, N.A., An approximate deconvolution procedure for large-eddy simulation, *Phys. Fluids*, **11** (7), p.1699-1701 (1999).

[21] Tadmor, E., Convergence of spectral methods for nonlinear conservation laws, *SIAM J. Numer. Anal.*, **26** (1), p.30-44 (1989).

[22] Xu, C.J. and Lin, Y.M., Open boundary conditions for the spectral simulation of Poiseuille-Benard flow, *Acta mechanica sinica*, **32(1)**, p1-10 (2000).

[23] Xu, C.J. and Pasquetti, R., On the efficiency of semi-implicit and semi-Lagrangian spectral methods for the calculation of incompressible flows, *Inter. J. Numer. Meth. Fluids*, **35**, p.319-340 (2001).

[24] Xu, C.J., A filter-based stabilization method of spectral element computations of high Reynolds number incompressible flows, *National congress of China on computational mathematics*, NanJing, China (2003).

APPENDIX

Here we give the details of the implementation of the elemental (i.e. before stiffness summation) "viscous stabilizing term" T_N. The approach described here follows what is usually done when a nodal basis is chosen.

The space $\boldsymbol{X}_N$ is first splitted into $\boldsymbol{X}_N^1$ and $\boldsymbol{X}_N^2$, $\boldsymbol{X}_N = \boldsymbol{X}_N^1 \oplus \boldsymbol{X}_N^2$, such that $\boldsymbol{X}_N^1$ (respectively $\boldsymbol{X}_N^2$) contains vectors with only the first (respectively the second) component non equal to zero.

Second, the Lagrangian basis is used to span $\boldsymbol{X}_N^1$ and $\boldsymbol{X}_N^2$, which vector fields may be assimilated to scalar fields.

Third, in each element $\Omega^k, k = 1, \cdots K$, the inner products are approximated by using the Gauss-Lobatto quadrature formula.

Let us focus on test-functions belonging to $\boldsymbol{X}_N^1$ and again denote $u_1 \in X_N^1$ and $v_1 \in X_N^1$ the first component of $\boldsymbol{u}_N$ and $\boldsymbol{v}_N$ respectively. The corresponding viscous term, say T_N^1, can be written:

$$T_N^1 = \nu \sum_{i,j=0}^{N} \left[F_1 S^{1/2}(\partial_X \tilde{u_1}) S^{1/2}(\partial_X \tilde{v_1}) + F_2 S^{1/2}(\partial_Y \tilde{u_1}) S^{1/2}(\partial_Y \tilde{v_1}) \right.$$
$$\left. + F_3 (S^{1/2}(\partial_X \tilde{u_1}) S^{1/2}(\partial_Y \tilde{v_1}) + S^{1/2}(\partial_Y \tilde{u_1}) S^{1/2}(\partial_X \tilde{v_1})) \right] (\xi_{ij}) \frac{\rho_{ij}}{J(\xi_{ij})}$$

where $\xi_{ij} = (\xi_i, \xi_j)$, $\rho_{ij} = \rho_i \rho_j$ with $\xi_i, \rho_i, i = 0, \cdots, N$ denoting the Legendre-Gauss-Lobatto points and corresponding weights in $[-1, 1]$. F_1, F_2, F_3 are three geometric factors, defined as

$$F_1 := (\partial_Y f_1)^2 + (\partial_Y f_2)^2 = J^2 \left[(\partial_y g_1)^2 + (\partial_x g_1)^2 \right]$$

$$F_2 := (\partial_X f_1)^2 + (\partial_X f_2)^2 = J^2 \left[(\partial_y g_2)^2 + (\partial_x g_2)^2 \right]$$

$$F_3 := -(\partial_X f_1 \partial_Y f_1 + \partial_X f_2 \partial_Y f_2) = J^2 \left[\partial_y g_2 \partial_y g_1 + \partial_x g_2 \partial_x g_1 \right]$$

where f_1 and f_2 (respectively g_1 and g_2) are the components of the mapping $\boldsymbol{f}$ (respectively $\boldsymbol{g}$).

Choosing now for each test function $v_1 \in X_N^1$ the Lagrangian polynomial h_{mn}, such that $h_{mn}(\xi_i, \xi_j) = \delta_{mi}\delta_{nj}$ (δ, Kronecker symbol) and expressing u_1 in this Lagrangian basis, we arrive at the matrix statement of T_N^1. For the element Ω^k, with u_{ij} for $u_1(\xi_i, \xi_j)$ and $D_S = S^{1/2} D$, where D is the usual

differentiation matrix:

$$T_N^1(m,n) = \nu \sum_{i=0}^{N} \frac{\rho_{in}}{|J(\xi_{in})|} F_{1,in} (D_S)_{im} \left(\sum_{p=0}^{N} (D_S)_{ip} u_{pn} \right)$$
$$+\nu \sum_{j=0}^{N} \frac{\rho_{mj}}{|J(\xi_{mj})|} F_{2,mj} (D_S)_{jn} \left(\sum_{q=0}^{N} (D_S)_{jq} u_{mq} \right)$$
$$+\nu \sum_{j=0}^{N} \frac{\rho_{mj}}{|J(\xi_{mj})|} F_{3,mj} (D_S)_{jn} \left(\sum_{p=0}^{N} (D_S)_{mp} u_{pj} \right)$$
$$+\nu \sum_{i=0}^{N} \frac{\rho_{in}}{|J(\xi_{in})|} F_{3,in} (D_S)_{im} \left(\sum_{q=0}^{N} (D_S)_{nq} u_{iq} \right) \quad , \forall m, n = 0, \cdots, N.$$

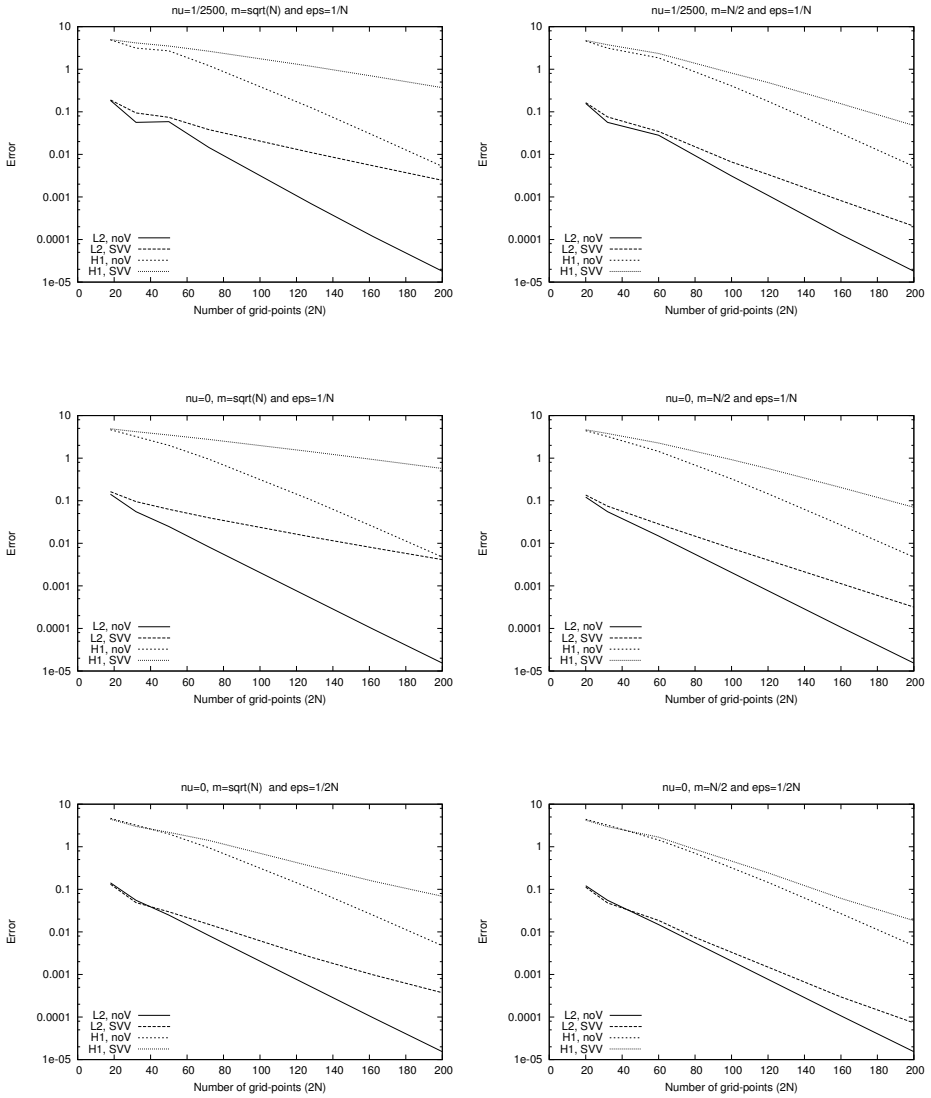

Figure 1: L^2 and H^1 norms of the error with and without spectral vanishing viscosity: $\nu = 1/2500$ for the 2 first diagrams and $\nu = 0$ elsewhere, $m_N = \sqrt{N}$ for the diagrams at left and $m_N = N/2$ for those at right, $\epsilon_N = 1/2N$ for the two last diagrams and $\epsilon_N = 1/N$ elsewhere.

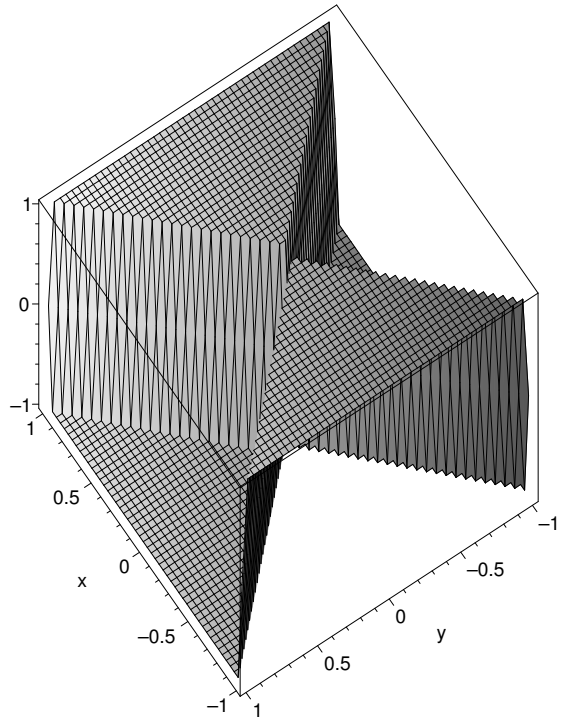

Figure 2: Exact analytical solution used in the 2D test.

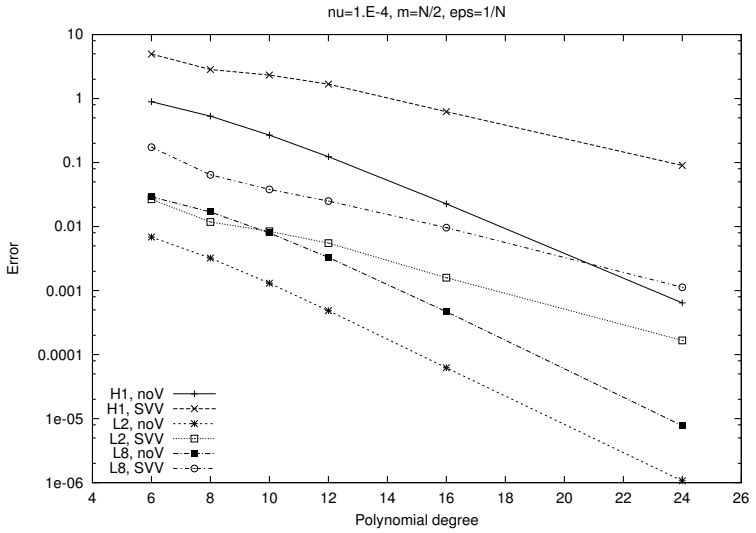

Figure 3: Errors of u in the H^1, L^2 and L^∞ norms vs the polynomial degree, obtained without SVV and with SVV ($\nu = 10^{-4}$, $m_N = N/2$ and $\epsilon_N = 1/N$).

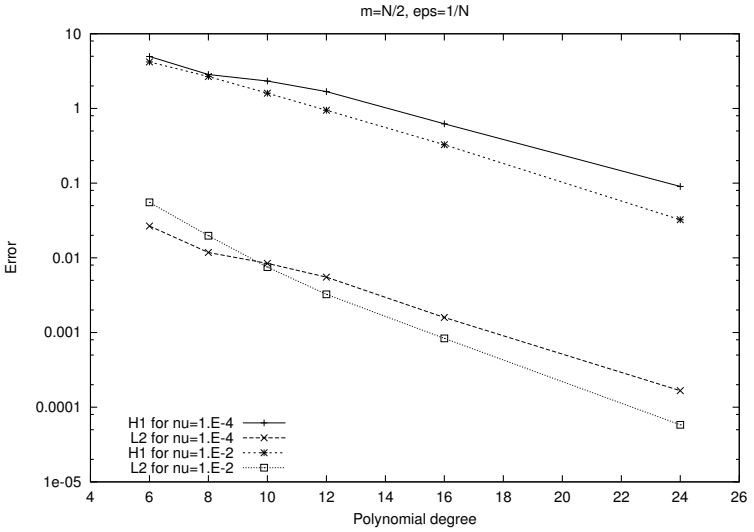

Figure 4: Errors of u in the H^1 and L^2 norms vs the polynomial degree for $\nu = 10^{-2}$ and $\nu = 10^{-4}$ ($m_N = N/2$ and $\epsilon_N = 1/N$).

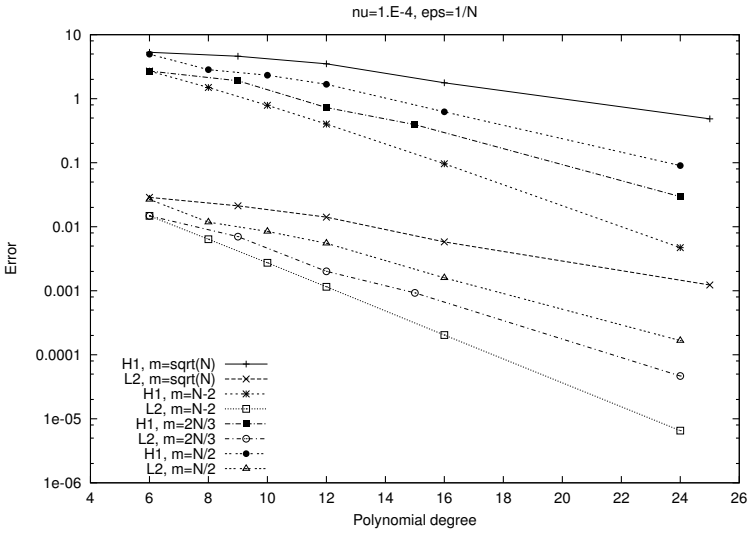

Figure 5: Errors of u in the H^1 and L^2 norms vs the polynomial degree for $m_N = \{\sqrt{N}, N-2, N/2, 2N/3\}$ ($\nu = 10^{-4}$ and $\epsilon_N = 1/N$) .

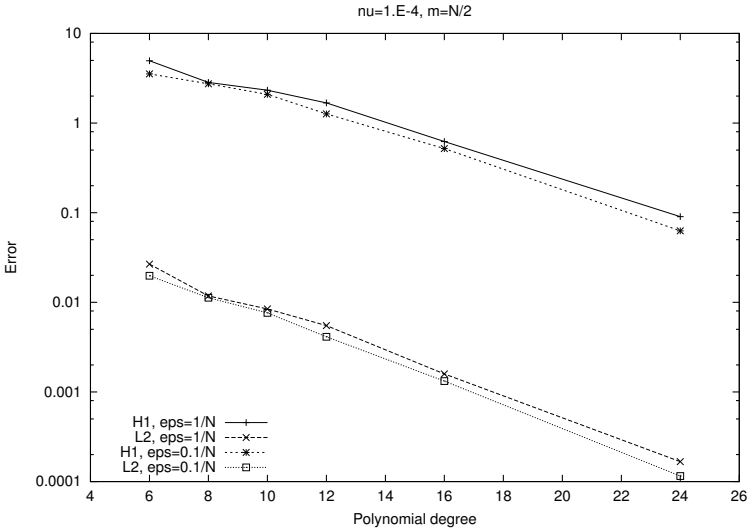

Figure 6: Errors of u in the H^1 and L^2 norms vs the polynomial degree for $\epsilon_N = 1/N$ and $\epsilon_N = 0.1/N$ ($\nu = 10^{-4}$ and $\epsilon_N = 1/N$).

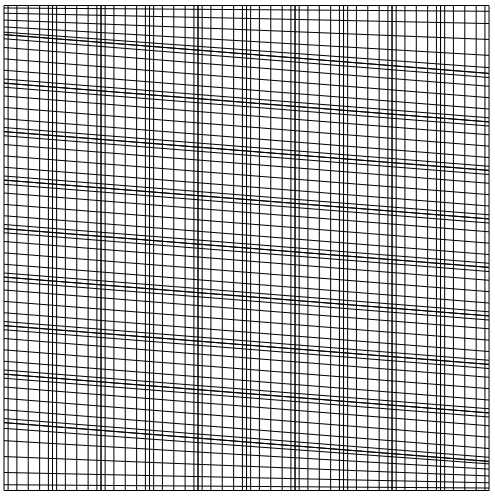

Figure 7: Deformed spectral element mesh.

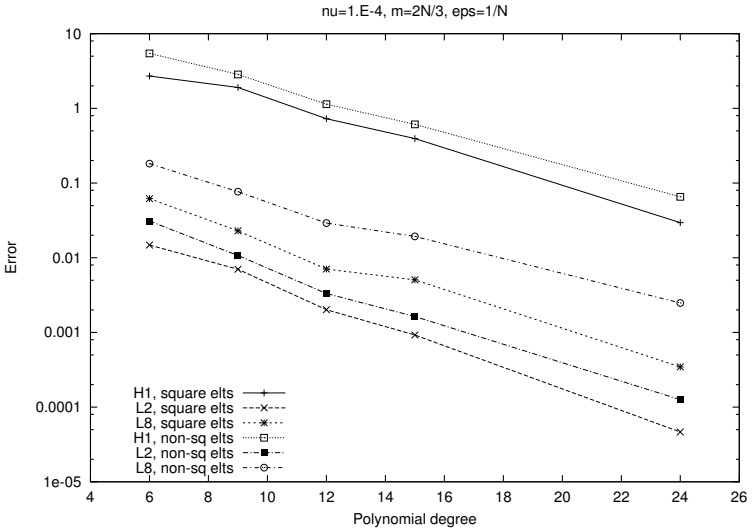

Figure 8: Errors of u in the H^1, L^2 and L^∞ norms vs the polynomial degree for different domain decompositions ($\nu = 10^{-4}, m_N = 2N/3, \epsilon_N = 1/N$).

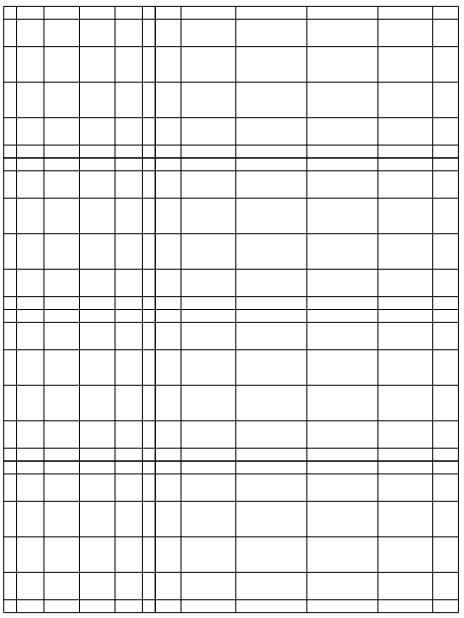

Figure 9: Spectral element mesh used to compute the Kovasznay flow

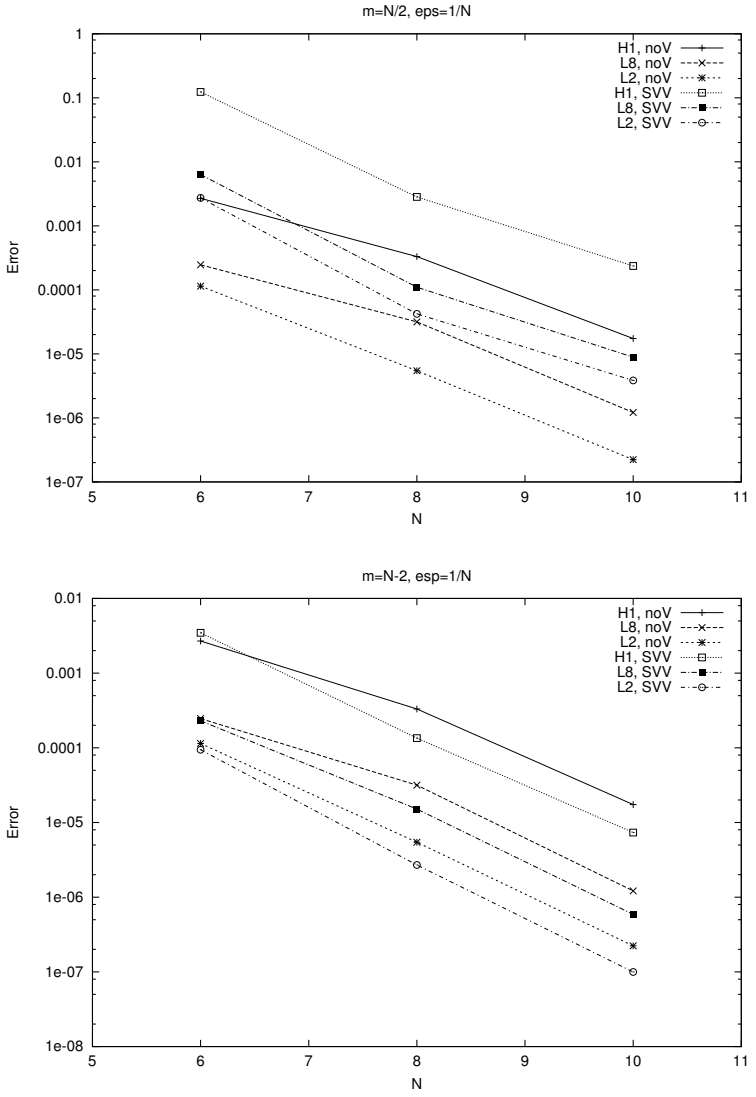

Figure 10: Kovasznay flow: Errors of $\boldsymbol{u}$ in the H^1, L^2 and L^∞ norms vs the polynomial degree for $m_N = N/2$ (top) and $m_N = N - 2$ (bottom) ($\epsilon_N = 1/N$).

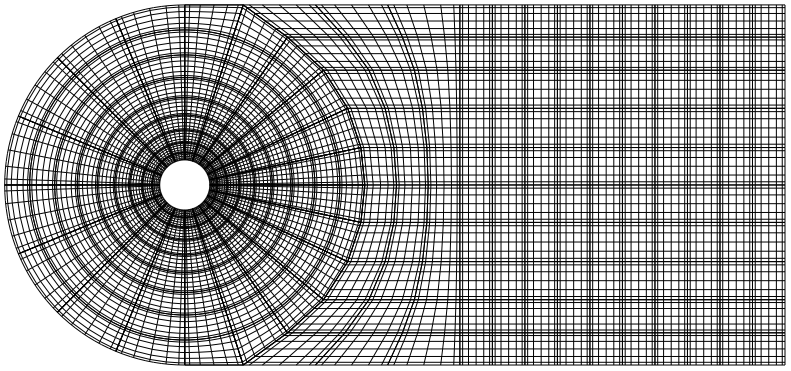

Figure 11: Spectral element mesh using 310 elements with 7×7 Gauss-Lobatto-Legendre grid-points. The height of the computational domain equals 7.2 and the distance from the cylinder axis to the outflow boundary equals 12.

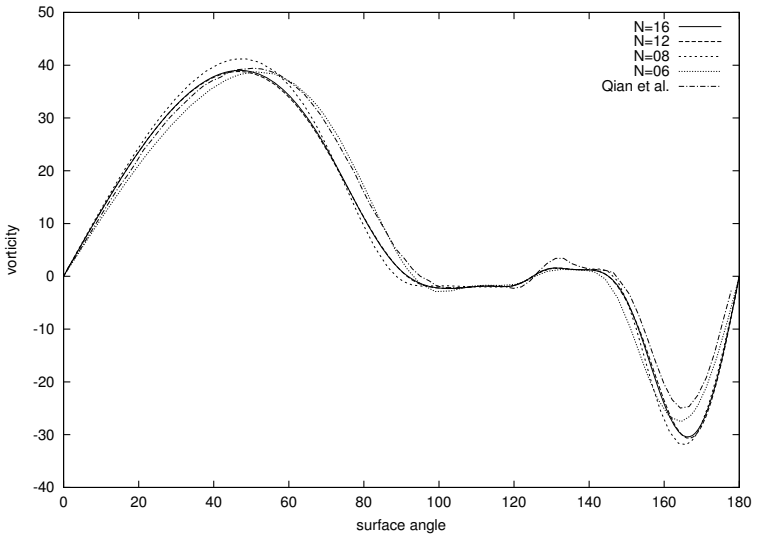

Figure 12: Surface vorticity distribution for different N with $m_N = 2N/3$ and $\epsilon_N = 1/N$ ($t = 6$, $Re = 1000$).

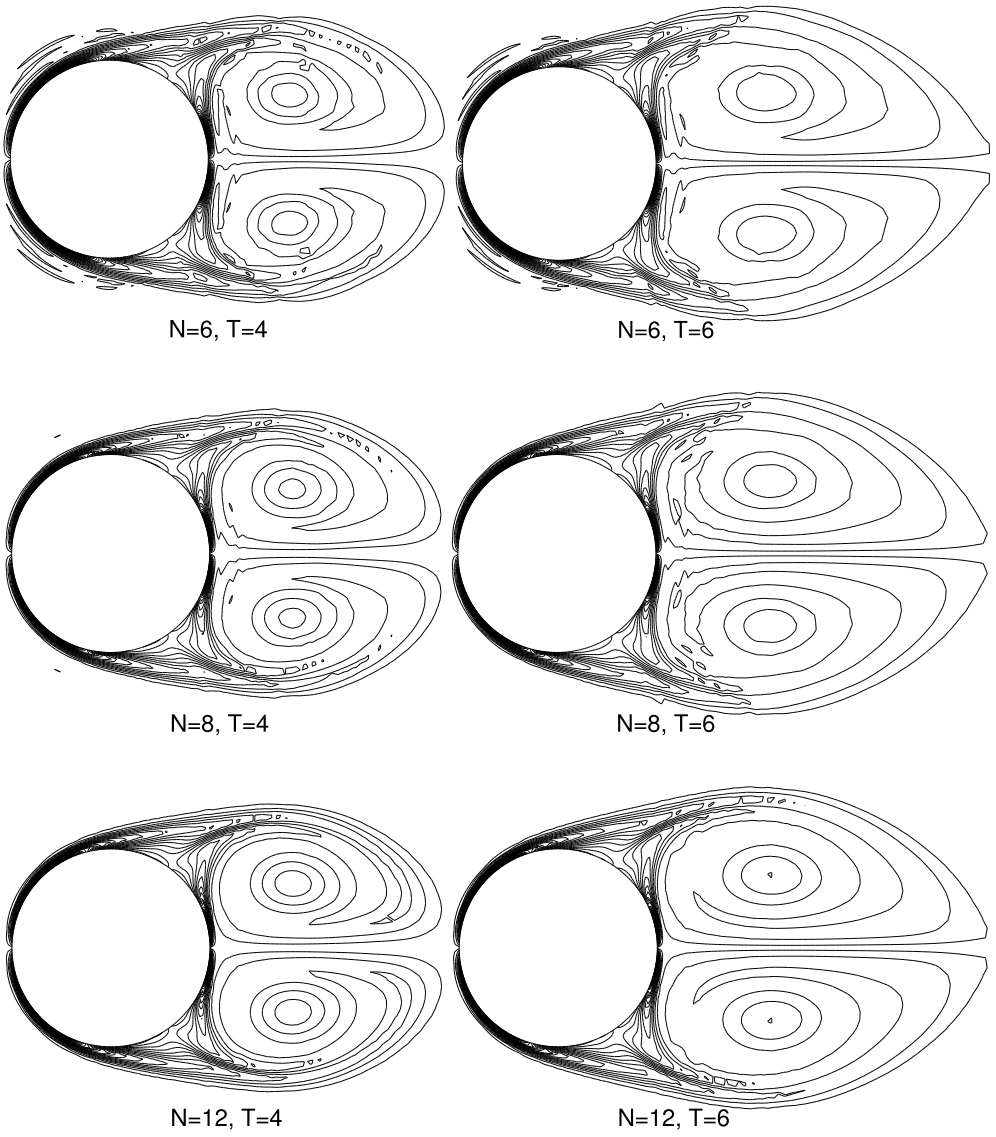

Figure 13: Vorticity isolines for different meshes, $N = \{6, 8, 12\}$ at times $t = 4$ at left and $t = 6$ at right ($Re = 1000$).

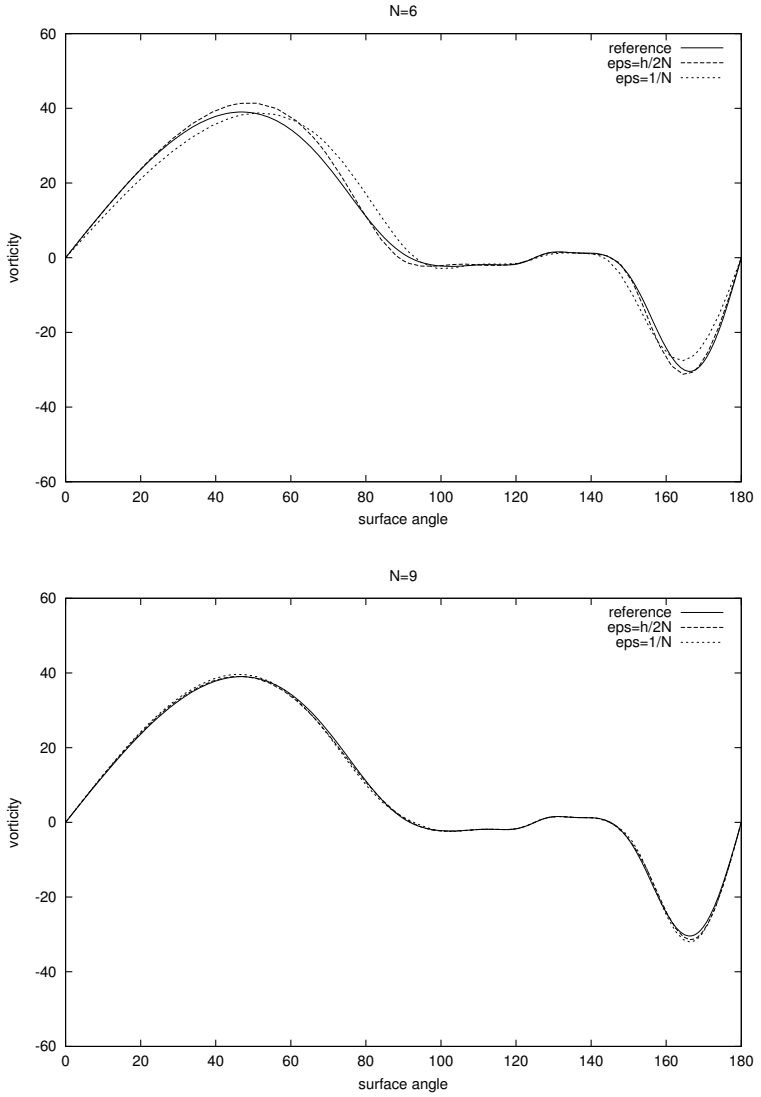

Figure 14: Surface vorticity distribution for $N = 6$ (top) and $N = 9$ (bottom), $\epsilon_N = h/2N$ and $\epsilon_N = 1/N$ with $m_N = 2N/3$ ($t = 6$, $Re = 1000$).

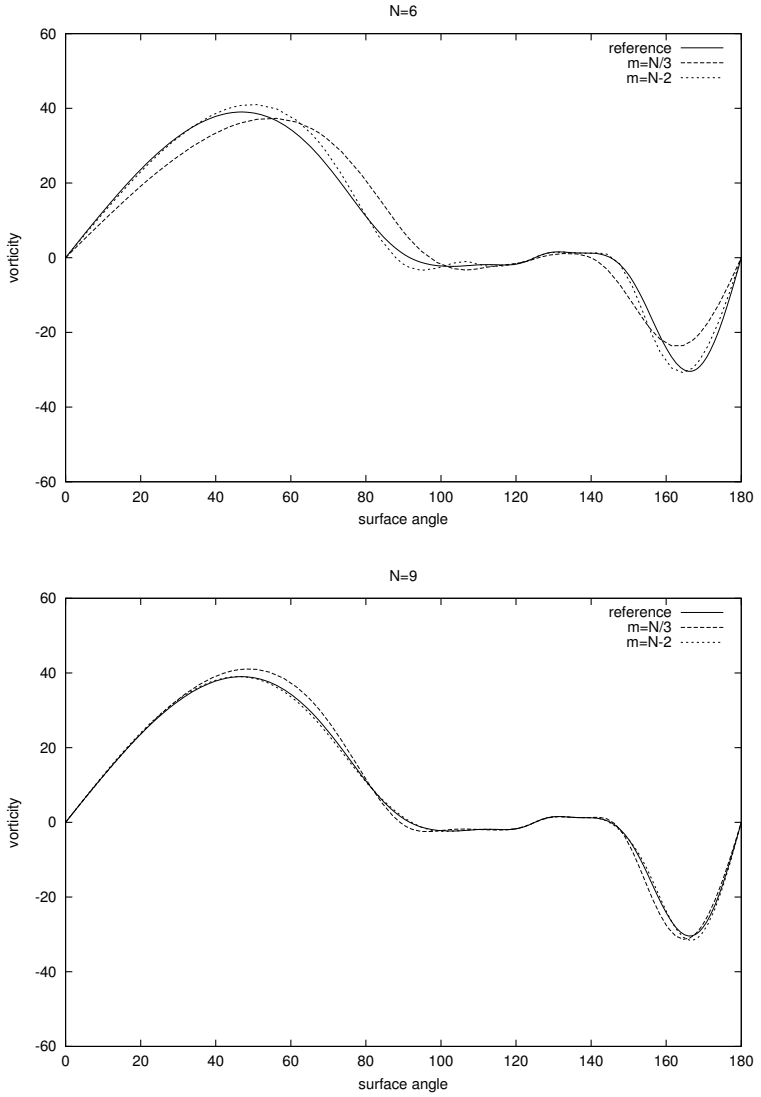

Figure 15: Surface vorticity distribution for $N = 6$ (top) and $N = 9$ (bottom), $m_N = N/3$ and $m_N = N - 2$ with $\epsilon_N = 1/N$ ($t = 6$, $Re = 1000$).

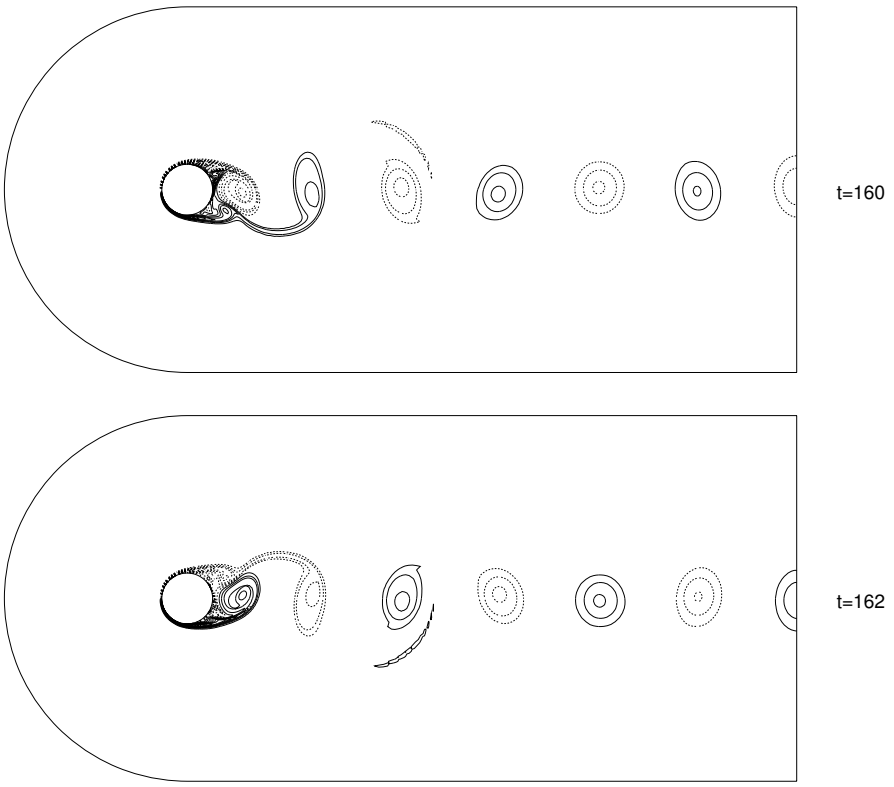

Figure 16: Vorticity contours for $Re = 1000$ at $t = 160$ and $t = 162$ using SVV-SEM with $\epsilon_N = 1/N$ and $m_N = N - 2$ (-104 $< \omega <$ 104, 80 equidistant levels).

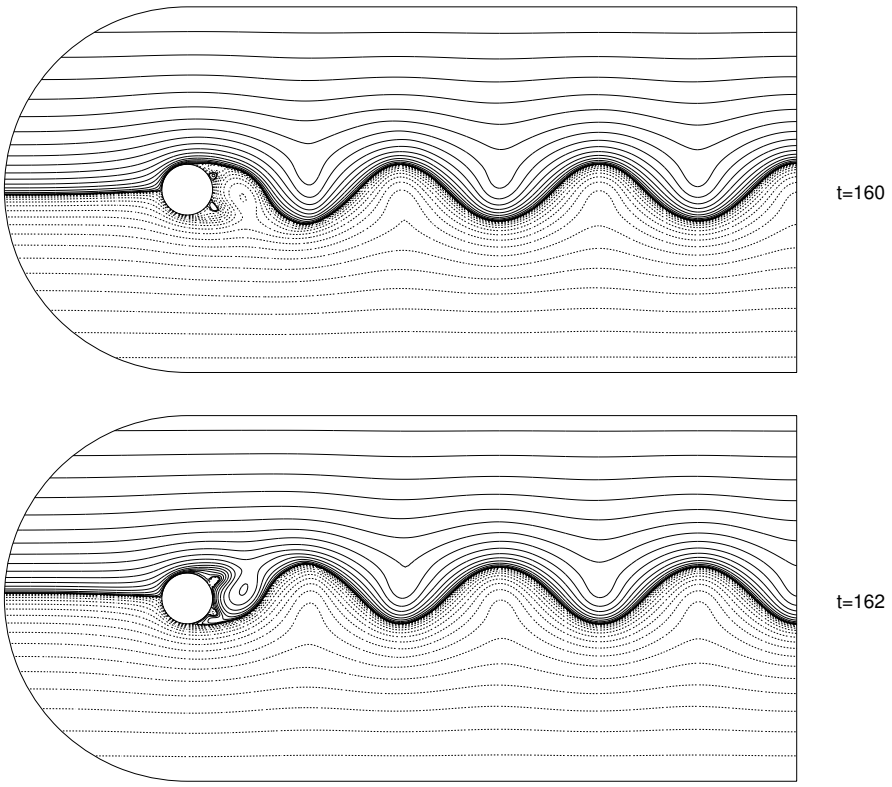

Figure 17: Streamlines for $Re = 1000$ at $t = 160$ and $t = 162$ using SVV-SEM with $\epsilon_N = 1/N$ and $m_N = N - 2$ (-3.75 $< \psi <$ 3.75, 40 non-equidistant levels with x^3 distribution).